Sputter-deposited $(Pb,La)(Zr,Ti)O_3$ thin films: Effect of substrate and optical properties

Ørnulf Nordseth,[a] Thomas Tybell, and Jostein K. Grepstad
Department of Electronics and Telecommunications, Norwegian University of Science and Technology (NTNU), NO-7491 Trondheim, Norway

Arne Røyset
SINTEF Materials and Chemistry, NO-7465 Trondheim, Norway

(Received 15 December 2008; accepted 16 March 2009; published 27 April 2009)

Optically transparent $(Pb,La)(Zr,Ti)O_3$ (PLZT) thin films were sputter-deposited on $SrTiO_3(001)$ and MgO(001) substrates with a $SrRuO_3(110)$ bottom electrode. X-ray diffraction analysis showed epitaxial growth of monocrystalline PLZT, with (001) rocking curve full width at half maxima of $\sim 0.03°$ and $\sim 0.3°$ for films deposited on $SrTiO_3$ and MgO, respectively. In-plane epitaxial alignment of the $SrRuO_3$ and PLZT epilayers was verified from φ-scans. It was established from atomic force microscopy measurements that the PLZT surface roughness meets the requirement for optical waveguide applications. Recorded *P-E* loops for films grown on both substrates showed a remanent polarization of $\sim 36\ \mu C/cm^2$. The refractive index of the PLZT layer was estimated from rutile prism coupling measurements at ~ 2.56 for $\lambda = 633$ nm, consistent with data obtained by spectroscopic ellipsometry. The ferroelectric and optical characteristics of the films, as well as their surface roughness, were not appreciably different for the two substrates. This makes MgO the preferred choice of substrate for optical waveguide devices due to its low refractive index compared to that of $SrTiO_3$. © *2009 American Vacuum Society.* [DOI: 10.1116/1.3117243]

I. INTRODUCTION

The large family of perovskite oxides offers a rich variety of functional properties,[1] such as pyro-, piezo-, and ferroelectricity, ferro- and antiferromagnetism, and electro-optic effect, which render these materials attractive for a wide range of device applications.[2–4] These include nonvolatile memory, ferroelectric field effect transistors, transducers, and sensors.[5,6] The transparent perovskite $(Pb,La)(Zr,Ti)O_3$ (PLZT) is recognized as a useful material for optical device applications, mainly by virtue of its low propagation losses at visible and near infrared wavelengths combined with a strong electro-optic response.[7] The addition of lanthanum to $Pb(Zr,Ti)O_3$ diminishes the optical anisotropy in the material,[8] resulting in substantially reduced light scattering for a La content in excess of 6 at. %.[9] The electro-optic characteristics of PLZT depend on the cation stoichiometry and may be classified as "linear," "quadratic," or "memory" according to the ferroelectric hysteresis behavior.[10,11] In this work, PLZT with 8% La substitution for Pb and a Zr:Ti cation ratio of 40:60 were chosen in order to obtain a linear electro-optic response (i.e., Pockels effect). A linear relation between refractive index and applied field is a prerequisite for electro-optic devices such as modulators and switches.[12]

The application of thin films in integrated optics places strict requirements on homogeneity and film thickness, as well as on surface morphology, to prevent losses from optical scattering.[13] Moreover, the electro-optic properties of thin films will be affected by the crystalline quality and orientation, residual stresses, grain boundaries, and the film-electrode interfaces.[14] In this study, we discuss epitaxial growth of $PLZT/SrRuO_3$ (SRO) bilayers on $SrTiO_3(001)$ and MgO(001) substrates using radio frequency (rf) magnetron sputtering. The thin SRO epilayer, grown prior to PLZT, was introduced to serve as bottom electrode for subsequent dielectric and ferroelectric measurements.[15] This planar electrode geometry renders a high electric field in the PLZT layer compatible with low-voltage operation, advantageous to electro-optic modulation. The $SrTiO_3$ substrate offers good lattice match with a wide selection of perovskite oxides. However, the relatively high refractive index of $SrTiO_3$ ($n = 2.38$) restricts the use of this substrate for thin film waveguide devices. MgO on the other hand has a low refractive index of $n = 1.74$, a prerequisite for strong optical mode confinement in the PLZT active layer. The MgO substrate has a larger lattice mismatch with PLZT, however, which tends to complicate epitaxial growth. This article analyzes and compares the crystalline, ferroelectric, dielectric, and optical properties of $Pb_{0.92}La_{0.08}Zr_{0.4}Ti_{0.6}O_3$ thin films grown on these two substrates.

II. EXPERIMENT

A. Thin film growth

Polished, (001)-oriented crystalline wafers of $SrTiO_3$ (Shinkosha Co., Ltd.) and MgO (MTI Crystal) were cut in $5 \times 5\ mm^2$ dies, cleaned ultrasonically in acetone, and subsequently rinsed with isopropyl alcohol. The substrates were fixed to a 2 in. diameter Inconel sample holder by silver paste, before introduction in the sputter chamber (Kurt J. Lesker Co.), equipped with Torus magnetron cathodes. The substrates were radiatively heated *in situ*, and their surface

[a]Electronic mail: ornulf.nordseth@iet.ntnu.no

 0734-2101/2009/27(3)/548/6/$25.00 ©2009 American Vacuum Society

temperature was measured using an optical pyrometer with the emissivity set at 0.7. The vacuum chamber base pressure was 5×10^{-8} Torr. The overall gas pressure was controlled with a manually operated gate valve, and the flow of Ar and O_2 (both of 99.9999% purity) was regulated by mass-flow controllers. The SRO and PLZT targets were both 3 in. diameter (Praxair, 99.9% purity), solder bonded to a copper alloy backing plate. The rf (13.56 MHz) power was 90 W for deposition of PLZT and 100 W for SRO.

The SRO epilayers were deposited in a 90° off-axis sputter geometry,[16] with a target center to substrate separation of ~100 mm. The layers were grown in a mixed ambient of O_2:Ar=4:10 at a total pressure in the growth chamber of 100 mTorr. The substrate temperature was ~630 °C. The typical thickness of the SRO electrode layer was 20 nm, as determined from x-ray reflectivity measurements,[17] and the deposition rate was approximately 0.4 nm/min. Prior to deposition of PLZT, the substrate temperature was lowered and stabilized within the range 490–570 °C, without breaking the vacuum. In order to achieve sufficient growth rates of films suitable for optical waveguide applications, i.e., with a typical thickness of 0.5 μm or more, the PLZT epilayers were deposited in a planar sputter geometry. The composition of the PLZT target was $Pb_{1.104}La_{0.08}Zr_{0.4}T_{0.6}O_3$, i.e., with 20 mol % excess lead to compensate for a disproportionate loss of lead from the film surface during deposition. The gun holding the PLZT target was mounted on a linear translator in order to allow for multilayer deposition. Optimum growth conditions for PLZT were established for a target-to-substrate separation of 48 mm. The films were grown in a mixed ambient of O_2:Ar=4:10 at total pressures of 100 and 165 mTorr for deposition on $SrTiO_3$(001) and MgO(001), respectively. The deposition rate under these conditions was approximately 2.5 nm/min. The samples were allowed to cool to room temperature in their growth ambient before being removed from the growth chamber.

B. Materials characterization

X-ray diffraction (XRD) measurements were carried out on a Bruker D8 Discover diffractometer to establish the phase and crystalline orientation of the individual thin film layers. The x rays were Cu $K\alpha$ (λ=1.54 Å) radiation, with the source operating at 40 kV and 40 mA. The film surface morphology was examined by tapping mode atomic force microscopy (AFM) using a Veeco Multimode V scanning probe microscope. The resonance frequency of the tips used was in the range 310–490 kHz, and the force constant varied between 22 and 91 N/m. The scan area was typically 5×5 μm^2, with a scan rate of 1 Hz. In order to investigate the ferroelectric and dielectric properties of the PLZT layers, circular Au(200 nm)/Pt(50 nm) top electrodes, 100 μm in diameter, were deposited on the perovskite thin film surface using e-beam evaporation. Polarization hysteresis and capacitance-voltage loops were measured on as grown films at 2 kHz with a small signal amplitude of 0.4 V using an Aixacct TF Analyzer 2000 system. The dielectric properties were analyzed for frequencies from 20 Hz to 1 MHz, at a bias level of 1 V_{rms}, with an HP 4284A Precision *LCR* meter.

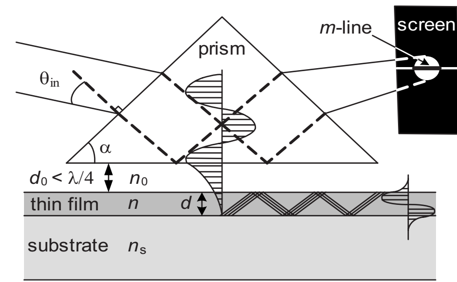

FIG. 1. Schematic of the prism-film coupler. The incident focused laser beam is totally reflected at the prism base. Wave guided modes in the optical thin film are excited selectively at certain angles of incidence, θ_{in}. The *m*-lines appearing on the detector screen are used to estimate numerically the thickness *d* and refractive index *n* of the optical thin film.

Polarized light from a λ=633 nm HeNe laser (Melles Griot 25-LHR-151) was coupled into PLZT layers with a thickness of ~650 nm, for films grown on both $SrTiO_3$ and MgO, without the SRO electrode layer, using an ADT-6 rutile prism pressed against the perovskite film surface. This setup, commonly referred to as a "prism-film coupler,"[18–20] is used to determine the thickness and refractive index of optically transparent thin films by running a numerical fit to the observed *m*-lines.[21] A schematic of the "prism-film coupler" is shown in Fig. 1. Light directed into the prism undergoes total reflection at the prism base. Reflected light emerging from the right face of the prism is projected onto a detector screen. Propagating optical modes are excited in the PLZT layer at certain angles of incidence θ_{in}, via overlapping evanescent fields,[18] i.e., provided the air gap d_0 between prism and film is less than $\sim\lambda/4$.[22] The energy losses associated with this excitation can be visually observed as a pattern of streaks (*m*-lines) on the detector screen, revealing the mode spectrum of the optical thin film. Complementary ellipsometric data for PLZT films grown on both $SrTiO_3$ and MgO was obtained using an MM-16 (Horiba Jobin Yvon) spectroscopic ellipsometer. The measurements were carried out with a 2 nm increment in wavelength over the full 430–850 nm range. The angle of incidence was 65°. A commercial software package (DELTAPSI2) was used to obtain a numerical fit to the recorded data, adopting the Levenberg–Marquardt nonlinear least-squares algorithm[23] and a single oscillator Sellmeier model for the refractive index dispersion,[24,25]

$$n^2(\lambda) - 1 = \frac{S_0\lambda_0^2}{1-(\lambda_0/\lambda)^2}, \quad (1)$$

where S_0 and λ_0 represent the average oscillator strength and position, respectively.

III. RESULTS AND DISCUSSION

A. Thin film crystalline structure and topography

Figures 2(a) and 2(b) display typical θ-2θ x-ray diffractograms of the PLZT/SRO bilayer for deposition on

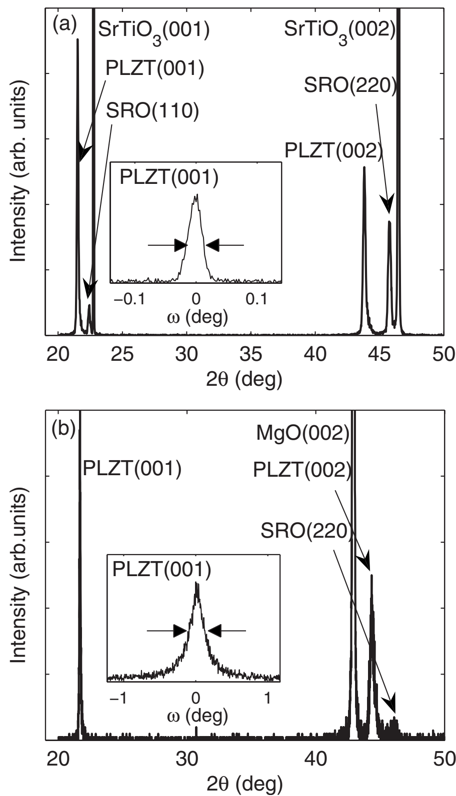

FIG. 2. θ-2θ scans of a PLZT/SRO bilayer grown on (a) $SrTiO_3(001)$ and (b) MgO(001). The diffractograms show purely (001)-oriented monocrystalline PLZT and (110)-oriented SRO on both substrates. The insets show the rocking curves for the PLZT(001) diffraction, with a FWHM of ~0.03° and ~0.3° for films grown on $SrTiO_3$ and MgO, respectively.

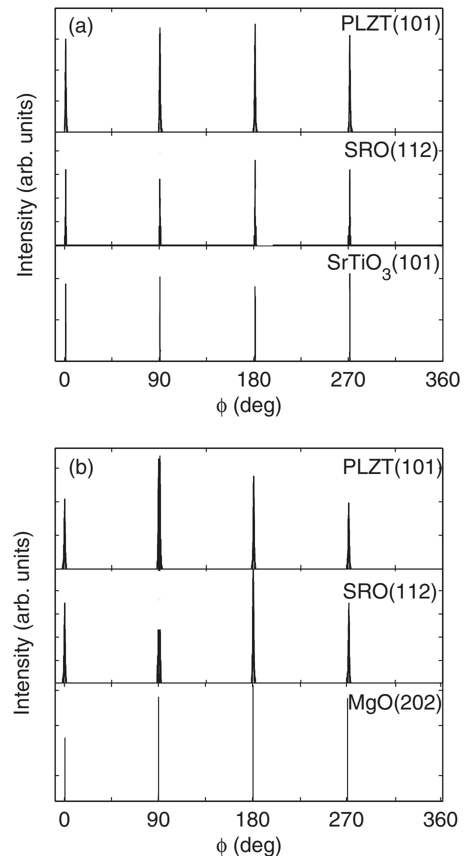

FIG. 3. φ-scans of a PLZT/SRO bilayer grown on (a) $SrTiO_3$ and (b) MgO. The observed fourfold symmetry verifies in-plane alignment of the PLZT and SRO layers.

$SrTiO_3(001)$ and MgO(001), respectively. The diffractograms show (110)-oriented SRO and (001)-oriented PLZT. For films grown on $SrTiO_3$, purely (001)-oriented perovskite PLZT was obtained for substrate temperatures in the range 490–570 °C. A pyrochlore phase was found to prevail for substrate temperatures below ~490 °C. For films grown on MgO, domains of different crystalline orientations were commonly observed, dependent on the substrate temperature as well as the overall gas pressure. In order to prevent the formation of pyrochlore for films grown on MgO, an increased ambient pressure of 165 mTorr was required, compared to 100 mTorr for films grown on $SrTiO_3$. Purely (001)-oriented PLZT could be grown on MgO at this total pressure (165 mTorr) for a limited range of substrate temperatures, $T_{sub}=550\pm 10$ °C.

For films grown on $SrTiO_3$, the rocking curve full width at half maximum (FWHM) for the PLZT(001) and SRO(110) diffraction peaks were measured at ~0.03°, comparable to that of the substrate (001) Bragg reflection. The FWHM of the corresponding rocking curves for PLZT and SRO deposited on MgO was measured at ~0.3° and ~1°, respectively. In Fig. 2, the rocking curve recorded for the PLZT(001) reflection is shown in the inset of each θ-2θ scan. The FWHM for PLZT on SRO/MgO(001) is comparable to that previously reported for deposition on CeO_2/YSZ-buffered Si(100) (Ref. 4) and smaller than that reported for the deposition on Pt/MgO(001).[26,27] The larger mosaic spread of PLZT and SRO grown on MgO, as compared to films grown on $SrTiO_3$, is attributed to the larger lattice mismatch with the substrate. For PLZT, these mismatches for growth on MgO and $SrTiO_3$ are 4.6% and 3.1%, respectively. The XRD data confirms that the crystalline quality of the PLZT film is not appreciably affected by incorporation of a thin SRO layer in the heteroepitaxial thin film stack. For PLZT grown on $SrTiO_3(001)$ without the SRO electrode layer, a minimum (001) rocking curve FWHM of ~0.03° was obtained for a substrate temperature of 530 ± 10 °C. For films grown at substrate temperatures above 550 °C the crystalline quality deteriorates, as judged from the rocking curve FWHM, presumably due to loss of Pb, as was previously observed with x-ray photoelectron spectroscopy for films deposited at elevated substrate temperatures.[4]

Figure 3 shows typical φ-scans for a PLZT/SRO bilayer grown on (a) $SrTiO_3(001)$ and (b) MgO(001). The fourfold symmetry of these azimuthal scans is evidence of in-plane alignment of the PLZT and SRO layers, with the [100] crystalline axis of PLZT parallel to that of the substrate.

Figure 4 shows a reciprocal space map of the PLZT/SRO bilayer on $SrTiO_3$. The recorded h and l coordinates of the (332) reflection for the orthorhombic SRO unit cell ($a=0.5532$ nm, $b=0.5572$ nm, $c=0.7850$ nm) (Ref. 28) imply that the SRO layer is compressively strained from isomor-

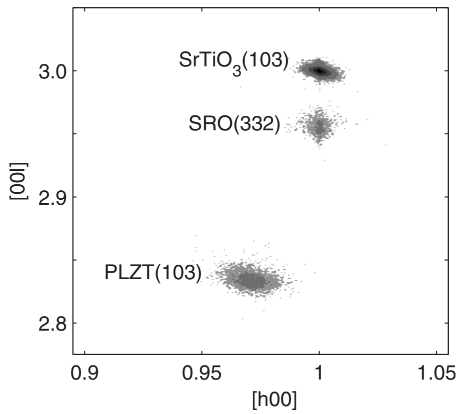

FIG. 4. Reciprocal space map of a PLZT/SRO bilayer on $SrTiO_3(001)$. The PLZT(103) peak is shifted by $\Delta h=0.029$ relative to that of the orthorhombic SRO(332) and $SrTiO_3(103)$ Bragg peaks.

phic growth on the $SrTiO_3$ substrate. The SRO unit cell will expand accordingly, perpendicular to the film surface. The recorded (220) diffraction from SRO at $2\theta=45.78°$ in Fig. 2(a) corroborates this finding. The measured 2θ angle corresponds to an out-of-plane lattice constant $c=0.3961$ nm, exceeding that of the pseudocubic lattice constant for bulk SRO (0.3928 nm) by approximately 1%. The reciprocal space map also shows that the PLZT(103) reflection is shifted relative to that of $SrTiO_3(103)$ by $\Delta h=0.029$. This translates into a PLZT in-plane lattice parameter of ~0.4020 nm, as compared to $a=b=0.4029$ nm for bulk $Pb_{0.92}La_{0.08}Zr_{0.4}Ti_{0.6}O_3$.[9] The PLZT(002) reflection at $2\theta=43.85°$ in Fig. 2(a) implies an out-of-plane lattice parameter $c=0.4126$ nm, consistent with the measured in-lattice parameters, to render a PLZT unit cell volume of 66.7 Å,[3] in good agreement with that of bulk $Pb_{0.92}La_{0.08}Zr_{0.4}Ti_{0.6}O_3$. Similar measurements for PLZT on MgO yielded in-plane and out-of-plane lattice parameters of $a=0.4021$ nm and $c=0.4108$ nm, respectively, suggesting partially relaxed growth of PLZT for these ~500 nm thick films also on the MgO substrate.

AFM scans of the PLZT/SRO bilayer showed that the root mean square (rms) surface roughness of the PLZT films increases with layer thickness for films grown on $SrTiO_3(001)$ and MgO(001) alike. For PLZT films 150, 300, and 500 nm thick, the rms surface roughness was measured at 0.9, 1.5, and 2.3 nm, respectively. Their surface roughness was not appreciably affected by the introduction of an SRO electrode layer. Hence, the surface roughness of films with sufficient thickness for optical waveguide applications meets the requirements for light propagation with moderate losses from surface scattering, (i.e., a rms surface roughness less than ~2–4 nm).[29] This suggests that the surface topography of the sputter-deposited PLZT films is adequate for application in optical waveguides and integrated optics. Inspection of the film surface with scanning electron microscopy shows uniform PLZT layers with no visible voids or cracks. Moreover, the measured surface roughness of ~80 nm thin PLZT layers grown by on-axis sputter deposition is comparable to that previously reported for films grown on $SrTiO_3(001)$ in the off-axis sputter geometry.[30] This observation suggests that the target geometry has little impact on the surface roughness of the sputter-deposited PLZT films.

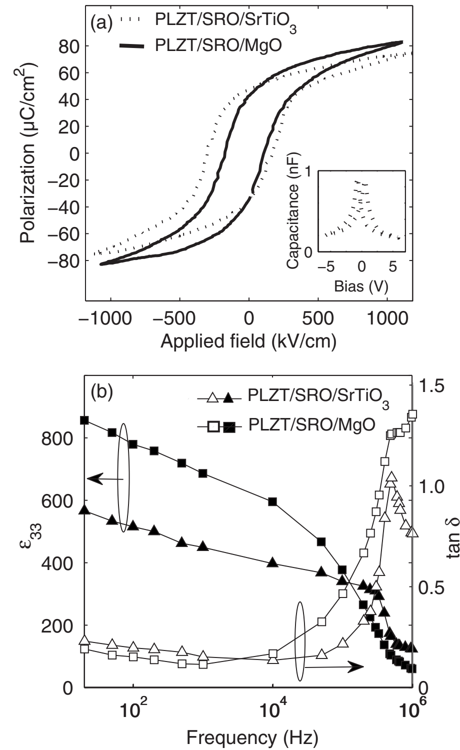

FIG. 5. (a) *P-E* hysteresis loops and (b) frequency responses of the dielectric constant ε_{33} (filled symbols) and the loss tangent tan δ (open symbols) for PLZT thin films grown on $SRO/SrTiO_3$ and SRO/MgO. The inset in (a) shows the measured *C-V* curve for the $PLZT/SRO/SrTiO_3$ sample.

B. Ferroelectric and dielectric measurements

The ferroelectric hysteresis behavior of PLZT films grown on $SRO/SrTiO_3$ and SRO/MgO is displayed in Fig. 5(a). The *P-E* loops show an average remanent polarization $P_r=36\ \mu C/cm^2$ and a coercive field $E_c=230$ kV/cm for PLZT on $SrTiO_3$ and corresponding values $P_r=36\ \mu C/cm^2$ and $E_c=140$ kV/cm for PLZT on MgO. The measured remanent polarization and coercive fields are larger than that previously reported for $Pb_{0.925}La_{0.075}Zr_{0.4}Ti_{0.6}O_3$ thin films ($26\ \mu C/cm^2$, 37 kV/cm) and bulk crystals ($28\ \mu C/cm^2$, 21 kV/cm).[31,9] The distinct hysteresis loops suggest that the sputter-deposited PLZT films are well suited for optical waveguide devices, for which a linear electro-optic response is desired. The inset in Fig. 5(a) shows the corresponding *C-V* switching curve for PLZT on $SrTiO_3$. We observe that the *P-E* and *C-V* loops are shifted toward a negative bias, as was previously reported for $Pb(Zr,Ti)O_3$ and PLZT thin films.[32,33] The different work functions for the Pt($q\Phi_m=5.5$ eV) (Ref. 34) and SRO($q\Phi_m=5.2$ eV) (Ref. 35) top and bottom electrodes contribute to this bias.[36,37] $\Delta\Phi_m$ cannot entirely account for the observed negative bias (~90 kV/cm), however. Trapped charges near the film-electrode interfaces and defects may also contribute to the observed bias shift.[38]

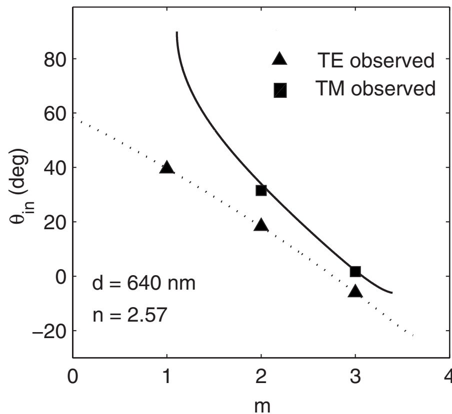

FIG. 6. Measured interdependence of the laser beam angle of incidence θ_{in} and the mode order m for rutile prism coupling measurements (cf. Fig. 1) of a PLZT thin film on MgO for TE and TM polarized light. The best fit for TE (dashed line) and TM polarization (solid line) suggests a refractive index $n=2.57$ and a film thickness $d=640$ nm for the actual wavelength of $\lambda=633$ nm.

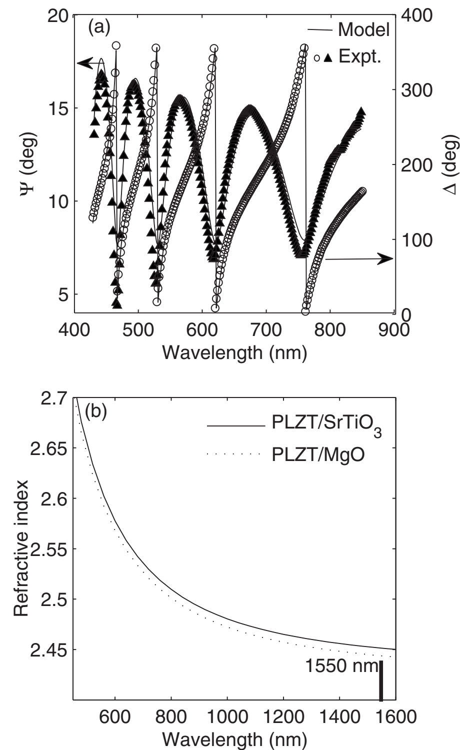

FIG. 7. (a) Spectrometric ellipsometry data (Ψ,Δ) with best fit from model calculations for a PLZT thin film on MgO. (b) Calculated dispersion of the refractive index for PLZT/$SrTiO_3$ and PLZT/MgO.

Figure 5(b) shows the room temperature dielectric frequency responses of PLZT grown on SRO/$SrTiO_3$ and SRO/MgO, respectively. The dielectric tensor component ε_{33} was estimated from the measured capacitance, assuming an ideal parallel-plate geometry. We note that for frequencies below 100 kHz, ε_{33} is larger for PLZT on MgO, as compared to films deposited on $SrTiO_3$ substrate. At 10 kHz, ε_{33} is measured at ~600 and ~400 for films grown on MgO and $SrTiO_3$, respectively. These values are comparable to the dielectric constant ($\varepsilon=982$) reported for bulk $Pb_{0.92}La_{0.08}Zr_{0.4}Ti_{0.6}O_3$.[9] The loss tangent (tan δ) is measured at ~0.2 for frequencies below 10 kHz and increases rapidly around 100 kHz for PLZT thin films grown on both substrates. Similar behavior was previously reported for capacitance measurements on PLZT, Pb(Zr,Ti)O_3, and (Pb,La)TiO_3 thin films[39,40] and attributed to a resonance in the measurement setup.[41]

C. Optical characterization

In Fig. 6, the laser beam angle of incidence θ_{in} (cf. Fig. 1) is plotted versus mode order for the observed m-lines of transverse electric (TE) and transverse magnetic (TM) polarized light coupled into a PLZT film grown on MgO substrate. The continuous curves in this plot are best fits from corresponding model calculations relating θ_{in} to mode order for TE and TM polarized light of $\lambda=633$ nm. The optically transparent thin film layer in this simulation had a film thickness of $d=640$ nm, refractive index of $n=2.57$, birefringence of $\Delta n=n_{TE}-n_{TM}=5\times10^{-3}$, and an opening angle of $\alpha=45°$ of the rutile prism. Corresponding fits to the m-lines observed for PLZT on $SrTiO_3$ rendered a refractive index $n=2.56$, consistent with that reported for bulk $Pb_{0.92}La_{0.08}Zr_{0.4}Ti_{0.6}O_3$ at $\lambda=633$ nm.[42] In these model calculations, the refractive index of the substrate was set at $n_s=2.38$ for $SrTiO_3$ and $n_s=1.74$ for MgO.[43,44]

Figure 7(a) shows the recorded ellipsometric parameters Ψ and Δ for the PLZT thin film on MgO, along with a numerical fit to the data. A surface roughness of 2 nm (rms) for the PLZT layer was implemented in the model, adopting an effective medium approximation.[45,46] The fit in Fig. 7(a) corresponds to $S_0=1.05\times10^{14}$ m^{-2} and $\lambda_0=215.1$ nm [Eq. (1)], which suggests a film thickness of ~650 nm and a refractive index $n\sim2.55$ for $\lambda=633$ nm, in good agreement with the data obtained from the prism coupling measurements. These values for the single Sellmeier oscillator match those previously reported for PLZT thin films.[47–49] Figure 7(b) shows the calculated dispersion of the refractive index for PLZT grown on $SrTiO_3$ and MgO for wavelengths spanning the 450–1600 nm range. We note that there is no major difference in the calculated dispersions for PLZT films on these two substrate materials. At the main communication wavelength of $\lambda=1550$ nm, the refractive index of the PLZT layer is $n\sim2.45$.

IV. CONCLUSIONS

PLZT(001) and SRO(110) thin films were grown epitaxially on $SrTiO_3$(001) and MgO(001) substrates by rf magnetron sputtering. The recorded rocking curves suggest that the PLZT epilayers are of good crystalline quality on both substrates. In-plane epitaxial alignment was confirmed from φ-scans, and the rms surface roughness was measured at ~2 nm for PLZT films of ~0.5 μm thickness, sufficient to meet the requirements for low-loss optical mode propagation in such films. The measured *P-E* hysteresis loops showed good ferroelectric behavior for films grown on both substrates, with a large coercive field and an average remanent

polarization of P_r=36 μC/cm^2. The dielectric constants (ε_{33}) at 10 kHz were measured at ~600 and ~400 for films deposited on MgO and $SrTiO_3$, respectively. Film thickness and refractive index were determined by rutile prism coupling and were found to be consistent with values derived from spectroscopic ellipsometry measurements. The dispersion of the refractive index was computed by means of a single oscillator Sellmeier model and was estimated at n ~2.55 for λ=633 nm and n~2.45 for λ=1550 nm for PLZT epilayers grown on both substrates. The ferroelectric and optical characteristics of these thin films, as well as their surface roughness, were not appreciably different for the two substrates. This finding favors MgO as the preferred choice of substrate for optical waveguide applications due to its low refractive index compared with $SrTiO_3$.

ACKNOWLEDGMENTS

This work was supported by The Research Council of Norway, under Project No. 158518/431, NANOMAT nationally coordinated project on "Oxides for Future Information and Communication Technology."

[1]M. E. Lines and A. M. Glass, *Principles and Applications of Ferroelectrics and Related Materials* (Clarendon, Oxford, 1979).
[2]R. Ramesh and N. A. Spaldin, Nature Mater. **6**, 21 (2007).
[3]J. F. Scott, Science **315**, 954 (2007).
[4]Ø. Nordseth, T. Tybell, and J. K. Grepstad, Thin Solid Films **517**, 2623 (2009).
[5]L. E. Cross, Ferroelectrics **76**, 241 (1987).
[6]M. Dawber, K. M. Rabe, and J. F. Scott, Rev. Mod. Phys. **77**, 1083 (2005).
[7]G. H. Haertling, Ferroelectrics **75**, 25 (1987).
[8]Y. J. Wu, J. Li, X. M. Chen, R. Kimura, and K. Kakegawa, J. Am. Ceram. Soc. **91**, 13 (2008).
[9]G. H. Haertling and C. E. Land, J. Am. Ceram. Soc. **54**, 1 (1971).
[10]G. H. Haertling, J. Am. Ceram. Soc. **54**, 303 (1971).
[11]J. M. Rouchon and F. Micheron, Czech. J. Phys. B, Sect. B **25**, 575 (1975).
[12]P. D. Thacher, Ferroelectrics **3**, 147 (1972).
[13]C. Ruppe and A. Duparré, Thin Solid Films **288**, 8 (1996).
[14]K. Nashimoto, S. Nakamura, T. Morikawa, H. Moriyama, M. Watanabe, and E. Osakabe, Jpn. J. Appl. Phys., Part 1 **38**, 5641 (1999).
[15]A. J. Hartmann, M. Neilson, R. N. Lamb, K. Watanabe, and J. F. Scott, Appl. Phys. A: Mater. Sci. Process. **70**, 239 (2000).
[16]J.-M. Triscone, L. Frauchiger, M. Decroux, L. Mieville, Ø. Fischer, C. Beeli, P. Stadelmann, and G.-A. Racine, J. Appl. Phys. **79**, 4298 (1996).
[17]L. G. Parratt, Phys. Rev. **95**, 359 (1954).
[18]P. K. Tien, R. Ulrich, and R. J. Martin, Appl. Phys. Lett. **14**, 291 (1969).
[19]J. H. Harris, R. Shubert, and J. N. Polky, J. Opt. Soc. Am. **60**, 1007 (1970).
[20]R. Ulrich and R. Torge, Appl. Opt. **12**, 2901 (1973).
[21]P. K. Tien and R. Ulrich, J. Opt. Soc. Am. **60**, 1325 (1970).
[22]P. K. Tien, Appl. Opt. **10**, 2395 (1971).
[23]D. W. Marquardt, J. Soc. Ind. Appl. Math. **11**, 431 (1963).
[24]M. DiDomenico, Jr. and S. H. Wemple, J. Appl. Phys. **40**, 720 (1969).
[25]S. H. Wemple and M. DiDomenico, Jr., Phys. Rev. B **3**, 1338 (1971).
[26]M. Kobune, O. Matsuura, T. Matsuzaki, A. Mineshige, S. Fujii, H. Fujisawa, M. Shimizu, and H. Niu, Jpn. J. Appl. Phys., Part 1 **39**, 5451 (2000).
[27]R. Wakabayashi, M. Kobune, T. Sawada, S. Kojima, and K. Honda, Integr. Ferroelectr. **46**, 27 (2002).
[28]R. J. Bouchard and J. L. Gillson, Mater. Res. Bull. **7**, 873 (1972).
[29]W. J. Leng, C. R. Yang, H. Ji, J. H. Zhang, H. W. Chen, and J. L. Tang, J. Appl. Phys. **100**, 083505 (2006).
[30]A. K. Sarin Kumar, Ø. Dahl, S. V. Pettersen, J. K. Grepstad, and T. Tybell, Thin Solid Films **492**, 71 (2005).
[31]M. Kobune, O. Matsuura, T. Matsuzaki, T. Sawada, H. Fujisawa, M. Shimizu, H. Niu, and K. Honda, Jpn. J. Appl. Phys., Part 1 **40**, 5554 (2001).
[32]J. Lee, C. H. Choi, B. H. Park, T. W. Noh, and J. K. Lee, Appl. Phys. Lett. **72**, 3380 (1998).
[33]G. E. Pike, W. L. Warren, D. Dimos, B. A. Tuttle, R. Ramesh, J. Lee, V. G. Keramidas, and J. T. Evans, Jr., Appl. Phys. Lett. **66**, 484 (1995).
[34]A. Goldmann, in *Condensed Matter*, Landolt-Börnstein, New Series, Group III, Vol. 23, edited by W. Martienssen (Springer-Verlag, Berlin, 2003),.
[35]C. Yoshida, A. Yoshida, and H. Tamura, Appl. Phys. Lett. **75**, 1449 (1999).
[36]Y. Lin, B. R. Zhao, H. B. Peng, Z. Hao, B. Xu, Z. X. Zhao, and J. S. Chen, J. Appl. Phys. **86**, 4467 (1999).
[37]V. C. Lo and Z. J. Chen, IEEE Trans. Ultrason. Ferroelectr. Freq. Control **49**, 980 (2002).
[38]D. Dimos, W. L. Warren, M. B. Sinclair, B. A. Tuttle, and R. W. Schwartz, J. Appl. Phys. **76**, 4305 (1994).
[39]S. K. Dey and J.-J. Lee, IEEE Trans. Electron Devices **39**, 1607 (1992).
[40]R. Thomas, S. Mochizuki, T. Mihara, and T. Ishada, Thin Solid Films **443**, 14 (2003).
[41]I. Polishchuk, G. Brown, and H. Huff, Rev. Sci. Instrum. **71**, 3962 (2000).
[42]P. D. Thacher, Appl. Opt. **16**, 3210 (1977).
[43]R. A. McKee, F. J. Walker, E. D. Specht, G. E. Jellison, L. A. Boatner, and J. H. Harding, Phys. Rev. Lett. **72**, 2741 (1994).
[44]K.-S. Hwang, C.-K. Kim, S.-B. Kim, J.-T. Kwon, J.-S. Lee, Y.-H. Yun, Y.-H. Kim, and B.-A. Kang, Surf. Coat. Technol. **150**, 177 (2002).
[45]D. A. G. Bruggeman, Ann. Phys. **24**, 636 (1935).
[46]D. E. Aspnes, Phys. Rev. B **41**, 10334 (1990).
[47]B. Tunaboylu, P. Harvey, and S. C. Esener, IEEE Trans. Ultrason. Ferroelectr. Freq. Control **45**, 1105 (1998).
[48]M. Okuyama, T. Usuki, Y. Hamakawa, and T. Nakagawa, Appl. Phys. (Berlin) **21**, 339 (1980).
[49]H. Li, Y. Zhang, J. Wen, S. Yang, D. Mo, C.-H. Cheng, Y. Xu, and J. D. Mackenzie, Jpn. J. Appl. Phys., Part 1 **39**, 1180 (2000).